NUMBER 1 OF 1

AUTHOR QUERIES

DATE 3/31/2009
JOB NAME JCLI
JOB NUMBER 0

ARTICLE jcli2472
QUERIES FOR AUTHORS NOTES AND CORRESPONDENCE

PLEASE ANSWER THE AUTHOR QUERIES WHERE THEY APPEAR IN THE TEXT.

AU1: This sentence is not clear. Have you rounded the c-c rate to 7%, or do the 12% of models have a rate of >7%, which is greater than the 6.5% c-c rate? I added ''approximately'' because I wasn't sure which you meant. Please clarify/edit as necessary.
AU2: In future, please limit abstract to 250 words per AMS style.
AU3: Please note that use of the first person (e.g., I/we/our) is not allowed in the abstract per AMS style. Please confirm edits.
AU4: Please update status.
AU5: Did not see any dashed black lines in latest version of Figure 3, so changed wording to gray shading. Also, there are three additional thicker vertical lines (at ~0.5, 1.1, and 1.8) in the P plots that are not explained.

JOBNAME: JCLI 00#0 2009 PAGE: 1 SESS: 8 OUTPUT: Tue Mar 31 20:32:59 2009 Total No. of Pages: 11
/ams/jcli/0/jcli2472

NOTES AND CORRESPONDENCE

Do Models and Observations Disagree on the Rainfall Response to Global Warming?

BEATE G. LIEPERT AND MICHAEL PREVIDI

Lamont-Doherty Earth Observatory of Columbia University, Palisades, New York

(Manuscript received 8 February 2008, in final form 23 September 2008)

ABSTRACT

Recently analyzed satellite-derived global precipitation datasets from 1987 to 2006 indicate an increase in global-mean precipitation of 1.1%–1.4% per decade. This trend corresponds to a hydrological sensitivity (HS) of 7% per kelvin of global warming, which is close to the Clausius–Clapeyron (CC) rate expected from the increase in saturation water vapor pressure with global warming. Analysis of two available global ocean evaporation datasets confirms this observed intensification of the atmospheric water cycle. The observed hydrological sensitivity over the past 20-yr period is higher by a factor of 5 than the average HS of 1.4% per kelvin simulated in state-of-the-art coupled atmosphere–ocean climate models for the twentieth and twenty-first centuries. However, the analysis shows that the interdecadal variability in HS in the models is high—in particular in the twentieth-century runs, which are forced by both increasing greenhouse gas (GHG) and tropospheric aerosol concentrations. About 12% of the 20-yr HS values of eight twentieth-century climate simulations from the third phase of the Coupled Model Intercomparison Project (CMIP3) have a magnitude greater than the CC rate of approximately 7% per kelvin. The analysis further indicates different HS characteristics for GHG and tropospheric aerosol forcing agents. Aerosol-forced HS is a factor of 2 greater, on average, and the interdecadal variability is significantly larger, with about 23% of the 20-yr sensitivities being above the CC rate. By thermodynamically constraining global precipitation changes, it is shown that such changes are linearly related to the difference in the radiative imbalance at the top of the atmosphere (TOA) and the surface (i.e., the atmospheric radiative energy imbalance). The strength of this relationship is controlled by the modified Bowen ratio (here, global sensible heat flux change divided by latent heat flux change). Hydrological sensitivity to aerosols is greater than the sensitivity to GHG because the former have a stronger effect on the shortwave transmissivity of the atmosphere, and thus produce a larger change in the atmospheric radiative energy imbalance. It is found that the observed global precipitation increase of 13 mm yr^{-1} per decade from 1987 to 2006 would require a trend of the radiative imbalance difference between the TOA and the surface of 0.7 W m^{-2} per decade. The recovery from the El Chichón and Mount Pinatubo volcanic aerosol injections in 1982 and 1991, the satellite-observed reductions in cloudiness during the phase of increasing ENSO events in the 1990s, and presumably the observed reduction of anthropogenic aerosol concentrations could have caused such a radiative imbalance trend over the past 20 years. Observational evidence, however, is currently inconclusive, and it will require more detailed investigations and longer satellite time series to answer this question.

1. Introduction

Changes in the global hydrological cycle associated with greenhouse gas–induced warming are one of the most important aspects of anthropogenic climate change. The common assumption is that global precipitation P will increase in a warmer world as a result of the strong temperature dependence of the water vapor saturation pressure e_s, as given by the Clausius–Clapeyron (CC) equation. For a global-mean surface temperature of 288 K (15°C), the CC equation predicts that e_s will increase by 6.5% per kelvin of surface warming.

Climate models (e.g., Allen and Ingram 2002) confirm an increase in the total amount of water vapor in the atmosphere at approximately the CC rate. Observations (e.g., Trenberth et al. 2005) indicate an increase of 1.3% ± 0.3% per decade from 1988 to 2001. With the earth's surface warming of 0.2 K per decade over the

Corresponding author address: Beate Liepert, Lamont-Doherty Earth Observatory, 61 Route 9W, Palisades, NY 10964.
E-mail: liepert@ldeo.columbia.edu

DOI: 10.1175/2008JCLI2472.1

same period (Trenberth et al. 2007), a rate of total water vapor increase of indeed 7% per kelvin is observed. Climate models, however, suggest that global-mean P increases at a much slower rate of about 1%–3% per kelvin of global warming (e.g., Held and Soden 2006). This discrepancy has been explained by either the thermodynamic energy constraints on the water cycle, which require global-mean P to change in accordance with the difference between the top of the atmosphere (TOA) and the surface radiative balance (see Mitchell et al. 1987; Boer 1993; Allen and Ingram 2002; Feichter et al. 2004), or by the dynamics of the Hadley circulation and extratropical moisture transport (Held and Soden 2006; Lorenz and DeWeaver 2007), which also dampen the global-mean P response to warming.

However, in a recent paper Wentz et al. (2007, hereinafter W07) state that over the last two decades global precipitation increased at close to the CC rate. This finding is based on satellite-derived global-mean P from Special Sensor Microwave Imager (SSM/I; version 6 that increased by 13.2 ± 4.8 mm per decade (1.4% ± 0.5% per decade) over the period from July 1987 through August 2006. The latest analysis of global-mean P from the Global Precipitation Climatology Project (GPCP; Adler et al. 2003; Gu et al. 2007) results in a smaller long-term trend of 3.8 mm per decade for the extended time period from 1979 to 2006 (Adler et al. 2008). However, Yin et al. (2004) generally urge caution when using GPCP and Climate Prediction Center Merged Analysis of Precipitation (CMAP; Xie and Arkin 1998) precipitation products for trend analysis prior to SSM/I in 1987—in particular over the oceans because of input data changes and atoll sampling in CMAP. The Intergovernmental Panel on Climate Change Fourth Assessment Report (IPCC AR4; Solomon et al. 2007) concludes that from 1979 to 2005 global precipitation trends range from −16 to +13 mm per decade for various datasets but that none of the trends are significant.

In accordance with other model studies, W07 found that decadal trends in P in the second Atmospheric Model Intercomparison Project (AMIP-II) climate model simulations (available online at http://www-pcmdi.llnl.gov/projects/amip) are smaller by a factor of 2–3 relative to the W07 observations for the 1987–2001 time period, even though these simulations are forced with observed sea surface temperatures. Allan and Soden (2007) further report of large discrepancies between observed (GPCP, CMAP, and SSM/I) and simulated precipitation trends of fully coupled climate models from phase 3 of the Coupled Model Intercomparison Project (CMIP3) in the ascending and descending branches of the tropical Hadley circulation. Increasing rainfall in the rising branch and decreasing trends in the descending regimes are detected in the observations for 1979–2006 [see also Chen et al. (2002), who confirm this feature], but these trends are not fully reproduced by the models. Both studies imply that the model–observation discrepancies in precipitation must be due to model parameterization errors and/or errors in the satellite data.

In this note, we focus on evaluating model performances on interdecadal time scales and argue that variability in climate-forcing agents such as aerosols and greenhouse gases (GHGs) on these time scales can play an important role in determining variability in observed and simulated global precipitation. We show that the strong increase in precipitation observed in the 1990s is not outside the CMIP3 models' range of interdecadal variability. Last, we discuss how the different effects of aerosols and GHGs on the TOA and surface radiation may explain variations in global precipitation, and we describe what role the Bowen ratio plays (the ratio of surface sensible heat flux to latent heat flux).

2. Data

Here we use two monthly mean precipitation products for calculating linear trends for the period from July 1987 to August 2006 and for the model comparisons: W07's merged product of ocean SSM/I and land GPCP data, and the GPCP product (Adler et al. 2003) for land and ocean precipitation. These global datasets have been analyzed before and are described in the introduction. Estimates of global ocean evaporation from synthesized surface meteorological conditions obtained from satellite remote sensing and atmospheric model reanalysis are also used. The evaporation products are the Objectively Analyzed Air–Sea Fluxes (OAFlux) for the global ice-free oceans by Yu and Weller (2007) and the Hamburg Ocean–Atmosphere Parameters and Fluxes from Satellite Data, version 3, (HOAPS3) by Andersson et al. (2007) for the oceans equatorward of 80° latitude. For both datasets, evaporation E at the ocean surface is calculated from the aerodynamic bulk formula based on Fairall et al. (2003) with wind speed, atmospheric specific humidity, and saturation specific humidity at sea surface as input data. The main difference of the datasets stems from the choice of input datasets and the preparation of the input data. OAFlux uses National Centers for Environmental Prediction and European Centre for Medium-Range Weather Forecasts reanalysis products and SSM/I, Quick Scatterometer, Advanced Very High Resolution Radiometer, Tropical Rainfall Measuring Mission Microwave Imager, and Advanced Microwave Scanning Radiometer for Earth Observing System satellite retrievals, whereas HOAPS3 relies only on SSM/I satellite

retrievals for the input parameters. For this study, we analyze *E* data for the time period from January 1987 to December 2004.

The model data used in our analysis are the global gridded monthly fields of *P* and surface air temperature (SAT) obtained for eight CMIP3 models {Geophysical Fluid Dynamics Laboratory Climate Model, version 2.0 (GFDL CM2.0); GFDL Climate Model, version 2.1 (GFDL CM2.1); Goddard Institute for Space Studies Model E-H (GISS-EH); Institute of Numerical Mathematics Coupled Model, version 3.0 (INM-CM3.0); Model for Interdisciplinary Research on Climate 3.2, high-resolution version [MIROC3.2(hires)]; MIROC3.2, medium-resolution version [MIROC(medres)]; Meteorological Institute of the University of Bonn ''ECHO-G'' Model (MIUBECHOG), and National Center for Atmospheric Research Community Climate System Model, version 3 (CCSM3)} for two different experiments, the ''climate of the twentieth century'' (20C3M) experiment and the Special Report on Emissions Scenarios A1B experiment. Both experiments were forced with observed (20C3M) or projected (A1B) changes in anthropogenic well-mixed greenhouse gases and aerosols. The 20C3M experiment also contains observationally based estimates of natural forcing resulting from changes in solar irradiance and volcanic activity. Because the initial conditions for the A1B experiment were taken from the end of the 20C3M experiment, continuous time series of *P* and SAT can be created for the entire twentieth and twenty-first centuries. Unlike the 20C3M and A1B experiments analyzed in this study, the AMIP-II experiments used by W07 did not apply any time-varying changes in atmospheric GHG, stratospheric and tropospheric aerosol concentrations, or solar irradiances. Yu and Weller (2007) conclude that these temporally variable forcings may affect moisture transport and evaporation. Thus, analysis of the 20C3M and A1B simulations provides an indication of whether modeled *P* changes during the past 20 years are sensitive to the specification of these time-varying forcings.

For the second part of the study, we analyze special simulations performed with the atmosphere model of the National Aeronautics and Space Administration (NASA) Goddard Institute for Space Studies coupled to the dynamic ocean model of Russell (GISS_ER). This model configuration was used for the IPCC AR4 (Solomon et al. 2007) and is described in detail by Hansen et al. (2007, hereinafter H07). The GISS_ER model was run with the IPCC AR4 transient forcings from 1880 to 2003. Different experiments were carried out with either all forcings applied simultaneously in the model or with each forcing applied individually (H07). The three experiments analyzed here are the ''tropospheric aerosols only'' experiment (trAerosols), the ''well-mixed greenhouse gases only'' experiment (GHG), and the experiment with all forcings applied at once. We show model results based on the multimember ensemble means from each of these experiments. Time-dependent tropospheric aerosols in the GISS_ER model are sulfate, black carbon, organic carbon, and nitrate. From 1880 onward, tropospheric aerosol optical depths increase nonlinearly—in particular, after 1950—similar to well-mixed greenhouse gases. After 1990 the tropospheric aerosol forcing is kept constant, whereas greenhouse gases continue to increase. Details of temporal and spatial distributions of these aerosols can be found in Koch (2001) and Hansen et al. (2005b, hereinafter H05). The indirect effect of aerosols on cloud coverage is parameterized as dependence of cloud coverage on the logarithm of concentrations of soluble aerosols. The total aerosol (effective) forcing, including the indirect effect on cloud coverage, is $F_e = -1.37$ W m^{-2} from 1880 to 2003. Well-mixed greenhouse gases in the model are carbon dioxide, methane, nitrous oxide, chlorofluorocarbons, and other trace gases. H07 report a GHG forcing of $F_e = 2.72$ W m^{-2} for 1880–2003, which is 2 times the magnitude of the aerosol forcing. The individual model runs for these and a variety of other forcing agents were available online at the time of writing (http://data.giss.nasa.gov/modelE/transient/climsim.html).

3. Interdecadal variability of global precipitation, evaporation, and temperature

Figure 1 shows the linear trends in global mean *P* and SAT for the eight models for the period from July 1987 through August 2006. Also shown are the observed *P* and SAT trends (dark gray bars) during this time period from SSM/I datasets (see W07) and the GPCP global precipitation trend (light gray shading) over the same period, which is slightly lower. We do not show the global *P* trend of −0.138% per decade of the CMAP dataset for the reasons discussed in the introduction. The figure also includes the GISS_ER trAerosol and GHG experiments, as well as the ''post Mount Pinatubo'' experiment, which represents the GISS_ER simulations, including all forcings, sampled here for the 12-yr period immediately following the Mount Pinatubo volcanic eruption in June of 1991. F1

It is obvious in Fig. 1 that all CMIP3 models underestimate the observed *P* increase of 1.40% ± 0.50% per decade for SSM/I and 1.14% ± 0.65% per decade for GPCP during the past 20 years despite the fact that six of the eight models simulate more surface warming than was observed. (Note the large uncertainty ranges of the observed *P* trends.) We assessed the statistical significance

JOBNAME: JCLI 00#0 2009 PAGE: 4 SESS: 8 OUTPUT: Tue Mar 31 20:33:00 2009 Total No. of Pages: 11
/ams/jcli/0/jcli2472

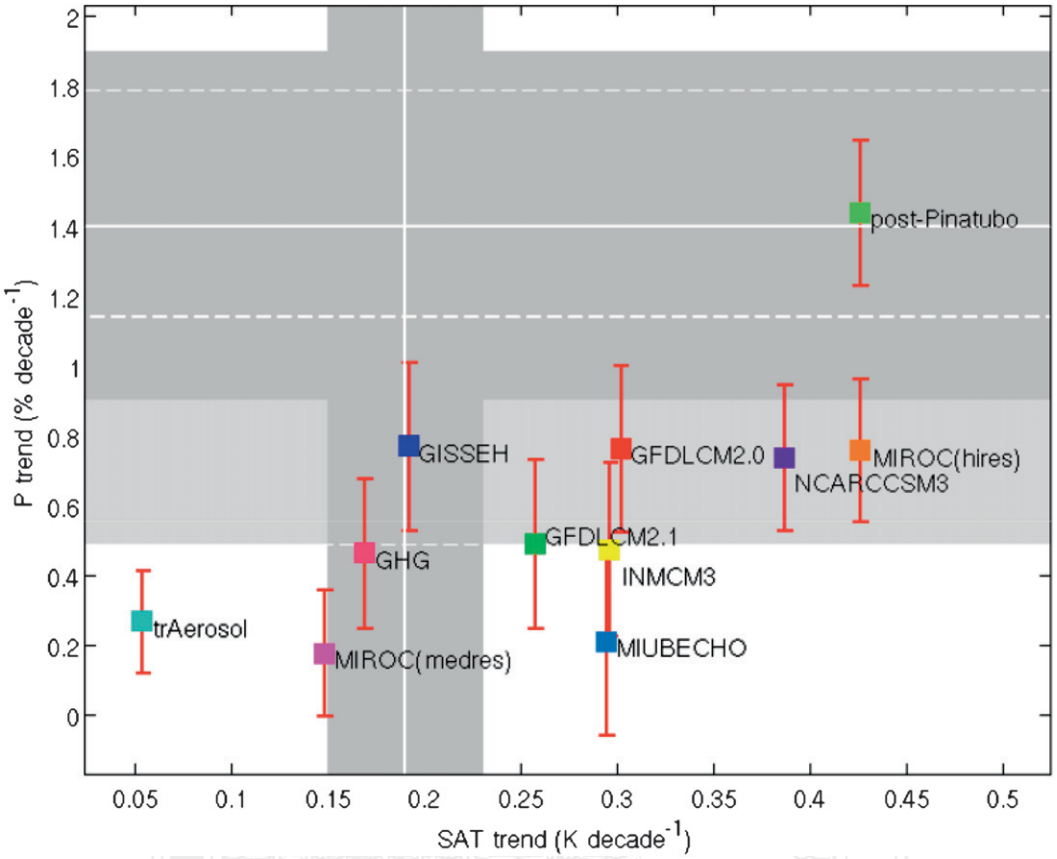

FIG. 1. Linear trends in global-mean *P* and SAT for the period from July 1987 through August 2006 based on the 20C3M and A1B simulations of the eight CMIP3 climate models, and linear trends in *P* and SAT for the period from 1987 through 2006 for three 20C3M-based simulations of the IPCC AR4 GISS_ER climate model—trAerosol is the experiment with temporarily changing anthropogenic aerosols forcing only, including aerosol indirect effects on clouds; GHG is the experiment with greenhouse gas forcing only; and "post Pinatubo" is the full 20C3M scenario but for period after the Mount Pinatubo volcanic eruption period in January 1992. Trends were calculated by performing a least squares linear regression on monthly-averaged model outputs after removing the seasonal variability. Error bars on the modeled *P* trends correspond to the 95% confidence level and account for autocorrelation of the regression error. The solid white horizontal (vertical) line is the best estimate of the observed trend in global-mean *P* (SAT) during the July 1987–August 2006 period, with the dark-gray shading indicating the associated uncertainty ranges (95% confidence). The dashed white lines and the light-gray shading are the corresponding *P* trend and uncertainty range (95% confidence) for the GPCP monthly mean precipitation dataset.

of the difference between observed and modeled *P* trends following Santer et al. (2000a,b) and found the difference to be significant at the 5% level for all models and the SSM/I dataset, but for only two of the eight models and the GPCP dataset. The ratio of the global-mean *P* trend to the global-mean SAT trend, referred to herein as the hydrological sensitivity (HS; e.g., Liepert et al. 2004), varies between 0.71% and 4.0% per kelvin for the eight models, with a multimodel mean of 1.9% per kelvin. The average HS is clearly smaller than the CC rate, and this result is in line with earlier work. Despite the large uncertainties of precipitation observations, several authors recognized the high interdecadal variability of observed global precipitation resulting from internal climate variability such as ENSO or external forcings such as major volcanic eruptions (Yin et al. 2004; Gu et al. 2007; Trenberth and Dai 2007; Trenberth et al. 2007). Gu et al. for example, estimate a contribution as high as a 5% reduction of tropical rainfall following several years after volcanic eruptions (Mount Pinatubo and El Chichón).

Figure 2 shows the global-mean anomalies of ocean surface evaporation from the OAFlux and HOAPS3 datasets for the slightly shorter time period from January 1987 to December 2004. The seasonality of *E* as well as *P* datasets was removed before the gridbox monthly mean anomalies were calculated. Evaporation anomalies over sea ice grid boxes in OAFlux and F2

JOBNAME: JCLI 00#0 2009 PAGE: 5 SESS: 8 OUTPUT: Tue Mar 31 20:33:20 2009 Total No. of Pages: 11
/ams/jcli/0/jcli2472

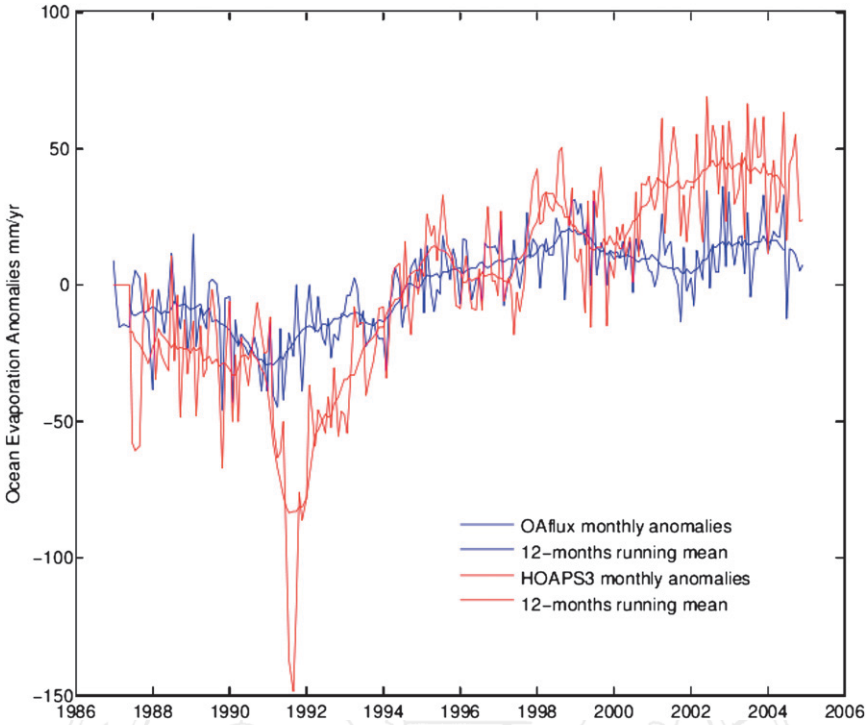

FIG. 2. Global monthly means of ocean evaporation anomalies from January 1987 to December 2004. The thick lines are the 12-month running means of the global and monthly mean anomalies. The OAFlux dataset is from the Woods Hole Oceanographic Institution and is for the global ice-free oceans, and the HOAPS3 dataset is from the Max-Planck Institute Hamburg and University of Hamburg and is for global oceans between 80°N and 80°S. The monthly anomalies time series are deseasonalized, and the ocean anomalies poleward of 80° are set to zero.

poleward of 80° in HOAPS3 are generally small relative to lower latitudes and were set to zero for this analysis. The 12-month running means (thick lines) indicate an upward tendency of the global ocean evaporation after a drop in 1991, which coincides with the Mount Pinatubo volcanic eruption in June of 1991. Evaporation drops dramatically in the HOAPS3 dataset following the Mount Pinatubo eruption but drops only slightly in OAFlux. Even after the Mount Pinatubo recovery, ocean evaporation after 2000 clearly exceeds the evaporation of the years before Mount Pinatubo in both datasets. The El Chichón volcanic eruption in March 1982 may have affected the beginning of the data as suggested by Gu et al. (2007). The main differences in E between the datasets may be due to the inclusion of reanalysis data in OAFlux, which do not account for the volcanic aerosol forcing and its full effects on dynamics and surface wind speed. HOAPS3 evaporation estimates only rely on SSM/I satellite retrievals of wind, humidity, and temperature fields, whereas OAFlux synthesizes reanalysis and satellite products of various sources. A more detailed investigation is needed to clarify these differences. We estimate a long-term increase in ocean evaporation of 18 ± 9 mm per decade and 51 ± 39 mm per decade from 1987 to 2004 for OAFlux and HOAPS3 based on a linear trend analysis. Note that the linear trend mainly reflects the low-frequency change and not the Mount Pinatubo dip particularly seen in HOAPS3. If no changes in evapotranspiration from land areas are assumed, the global-mean trends of evaporation solely based on ocean changes would be 16 ± 8 mm per decade and 45 ± 35 mm per decade for OAFlux and HOAPS3, respectively. (We note that ocean evaporation is about a factor of 6 larger than evapotranspiration from land.) Thus, OAFlux evaporation changes without land contribution compare favorably to the global-mean P increase of 13 ± 5 mm per decade from 1987 to 2006 (W07), whereas HOAPS3 changes would likely require reductions of evapotranspiration from land to match the observed global P trends. However, both E datasets are consistent with the observed P increase to within their respective uncertainty ranges.

Apart from the uncertainties in the global observational data, the discrepancies between global-mean modeled and observed P changes as shown in Fig. 1 during the past 20 years lead one to question how well the interdecadal

JOBNAME: JCLI 00#0 2009 PAGE: 6 SESS: 8 OUTPUT: Tue Mar 31 20:33:39 2009 Total No. of Pages: 11
/ams/jcli/0/jcli2472

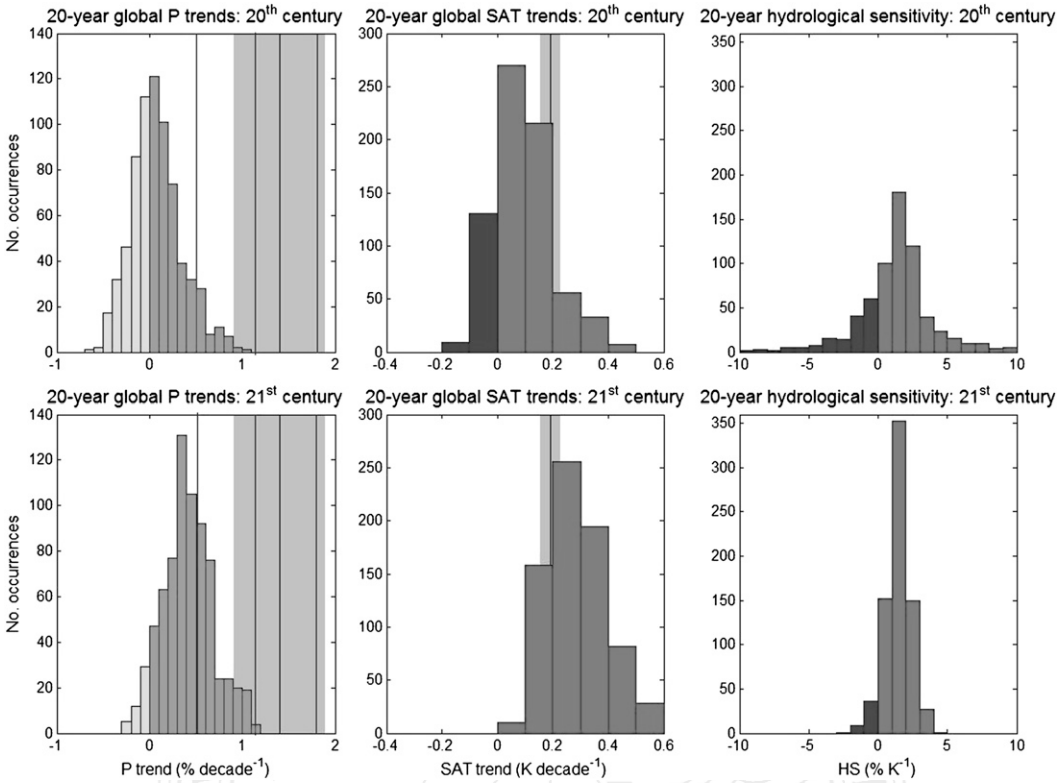

FIG. 3. Distributions of 20-yr linear trends in global-mean (left) *P* and (middle) SAT for the eight CMIP3 climate models listed in Fig. 1 for the twentieth and twenty-first centuries. Also shown are the associated distributions of (right) HS, defined as the 20-yr *P* trend divided by the 20-yr SAT trend. Trends in *P* and SAT were calculated by performing a least squares linear regression on monthly-averaged model output after removing the seasonal variability. The distributions for the twentieth century are based on 90 overlapping 20-yr periods (i.e., the first 20-yr period is 1900–19, the second is 1901–20, and the last is 1989–2008); those for the twenty-first century are based on 91 overlapping 20-yr periods (i.e., the first 20-yr period is 1990–2009 and the last is 2080–99). This yields a total of 720 samples (ninety 20-yr periods × eight models) for each of the three twentieth-century distributions, and 728 samples for the twenty-first-century distributions. The thin vertical solid lines in the *P* and SAT distributions correspond to the best estimates of the observed trends in global-mean *P* and SAT during the July 1987–August 2006 period, with the surrounding gray shading showing the associated uncertainty ranges (95% confidence).

AU5

variability of global-mean *P* or *E* is reproduced in models and how this interdecadal variability will change in the future in response to anthropogenic forcing.

Here we examine the interdecadal variations in *P* in the CMIP3 climate models to evaluate the likelihood of a 7% global *P* increase per kelvin, as recently observed in the 20-yr SSM/I merged satellite product. Linear trends in global-mean *P* for overlapping 20-yr periods in the twentieth and twenty-first centuries are calculated. F3 Figure 3 shows the combined (i.e., for all eight models) distributions of *P* trends along with distributions of global-mean SAT trends and the hydrological sensitivities based on these trends. The mean 20-yr global *P* and SAT trends are 0.076% per decade and 0.093 K per decade in the twentieth century and increase considerably to 0.41% per decade and 0.28 K per decade in the twenty-first century. For comparison, the multimodel mean global *P* and SAT trends for the period from July 1987 through August 2006 (see Fig. 1) are 0.55% per decade and 0.29 K per decade, respectively. Thus, this recent 20-yr period in the models is anomalous in terms of its relatively rapid rate of *P* increase when compared with the mean rate of *P* increase during the twenty-first century, even though the corresponding rates of surface warming are very similar. It is evident from Fig. 3 that several 20-yr periods in both the twentieth and twenty-first centuries are characterized by *P* trends falling within the uncertainty range of the observed *P* trends in Fig. 1. Model-simulated trends are as large as the best estimate of 1.14% per decade of GPCP but are not as large as the best estimate of 1.40% per decade of the SSM/I precipitation trend.

The above results indicate that 20-yr increases in global *P* close to the observed increases are not outside

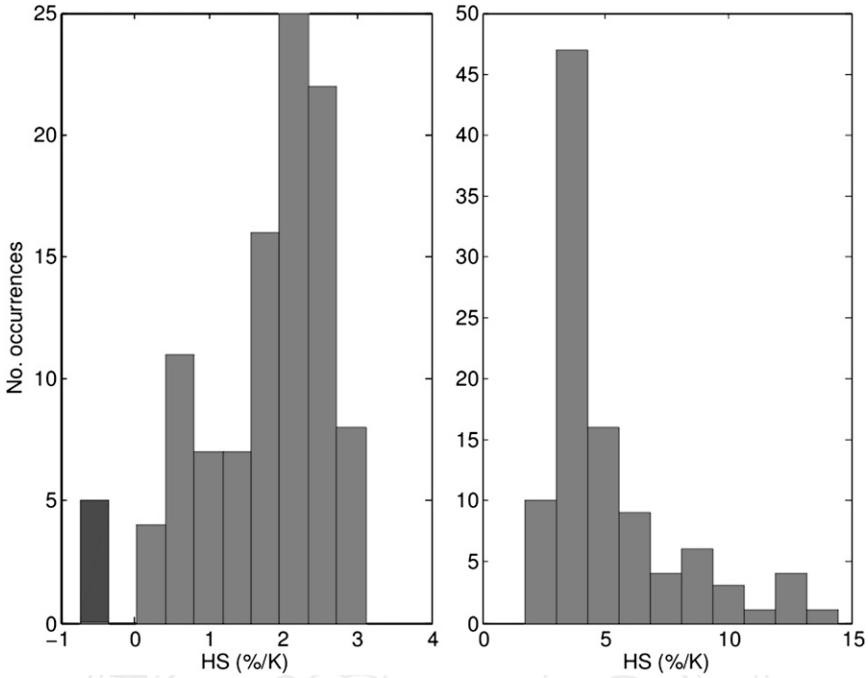

FIG. 4. Distributions of 20-yr linear trends in global-mean *P* and SAT for (left) the GHG simulations with greenhouse-gases forcing only and (right) the trAerosol simulations with tropospheric aerosol only for the twentieth-century ensemble simulations of the GISS_ER climate model (H05), illustrated by showing the associated distributions of HS, defined as the 20-yr *P* trends divided by the 20-yr SAT trends. Trends in *P* and SAT were calculated by performing a least squares linear regression on monthly-averaged ensemble-mean model output after removing the seasonal variability. The distributions for the twentieth century are based on 104 overlapping 20-yr periods beginning with 1880–99 and ending with 1984–2003.

the models' range of interdecadal variability, albeit the simulated mean trend is considerably smaller. Such relatively large *P* increases occur in the models because of some combination of internal climate variability, interdecadal variability in forcing, and/or climate response to forcing. The latter will be investigated below. Figure 3 also indicates that several 20-yr periods of decreasing global *P* are predicted to occur by the models in the twenty-first century despite the fact that all 20-yr periods in the century show increasing SAT. That global *P* can decrease in a warming world has been suggested previously (Liepert et al. 2004) as a consequence of anthropogenic aerosol emission increases.

The distributions of HS shown in Fig. 3 reveal notable differences between the twentieth and twenty-first centuries. Although the median 20-yr HS is the same in both centuries, being about 1.4% per kelvin, the spread of the HS distribution is significantly greater during the twentieth century. (Note that the median rather than the arithmetic mean is used as an indication of the average 20-yr HS because of the presence of large-magnitude outliers in the distribution.) Approximately 12% of the HS values in the twentieth century have a magnitude that is greater than the increase in moisture holding capacity (CC rate of 6.5% per kelvin). These large-magnitude HS values are generally associated with very small magnitude trends in global-mean SAT. For example, for the periods with an HS larger in magnitude than the CC rate, the mean absolute value of the 20-yr SAT trend is only 0.017 K per decade. In the twenty-first century, as global warming accelerates, these small-magnitude SAT trends are reduced considerably in number and the HS distribution narrows (see Fig. 3). The entire twenty-first-century HS distribution is within plus or minus the CC rate.

4. Hydrological sensitivity to GHG and tropospheric aerosol forcings

We expect that differences in the width of the HS distributions between the twentieth and the twenty-first century arise partly as a result of differences in the forcings and their climate feedbacks. The A1B (twenty-first century) scenario is dominated by increasing well-mixed greenhouse gases, whereas in the twentieth-century forcing scenario increases in GHGs are accompanied by

JOBNAME: JCLI 00#0 2009 PAGE: 8 SESS: 8 OUTPUT: Tue Mar 31 20:33:50 2009 Total No. of Pages: 11
/ams/jcli/0/jcli2472

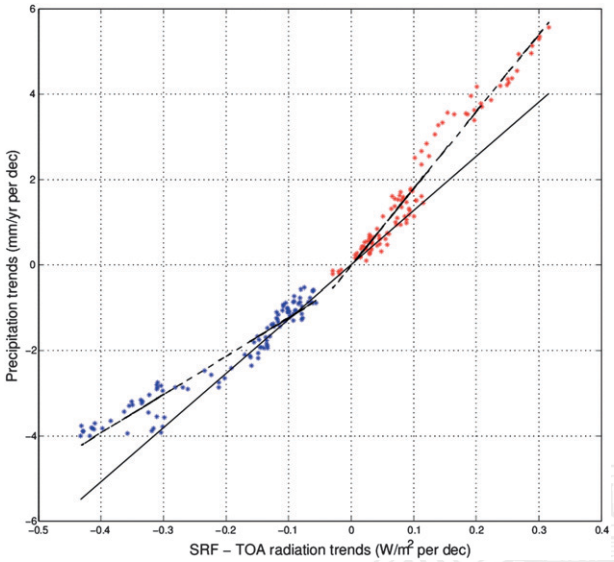

FIG. 5. Scatter diagram of modeled 20-yr linear trends in global precipitation vs corresponding linear trends of surface-minus-TOA global net radiation fluxes. The model data are twentieth-century ensemble simulations of the GISS_ER climate model (H05) for the GHG scenario (red asterisks) and trAerosol scenario (blue asterisks) for the time period from 1880 to 2003. The regression lines are based on least squares estimates. Regressions were calculated for the combination of the GHG and trAerosol datasets (solid line) and for the GHG and trAerosol experiments individually (dashed lines). The data points of linear trends were calculated for 20-yr overlapping time periods beginning with 1880–99 and ending with 1984–2003. The global-mean linear trends of precipitation and net radiation differences are calculated from monthly anomalies after removing the seasonal variability.

other forcings, predominantly rising aerosol concentrations (H07). Different HS to aerosol and greenhouse gas forcings exemplifies the different P responses to shortwave (SW) and longwave (LW) forcings. Gillett et al. (2004) detected the influence of volcanic aerosols on observed global precipitation and concluded that "shortwave forcings exert a larger influence on precipitation than longwave forcings."

Here we assess the difference in HS to aerosol and greenhouse gas forcing agents. The trend analysis for 20-yr overlapping periods is repeated with results from the GISS_ER GHG and trAerosol experiments. As expected, the average global P trend of 0.31% per decade and SAT trend of 0.16 K per decade for the GHG experiment are smaller than the corresponding trends for the twenty-first-century scenario (A1B) but are substantially higher than the twentieth-century 20C3M simulations that include all forcings (see section 2). In contrast to GHG, increasing tropospheric aerosols in the trAerosol scenario exert a small mean cooling trend of −0.085 K per decade and a mean decrease in global P of −0.39% per decade. The median hydrological sensitivity of 4.1% per kelvin (mean of 5.1% per kelvin) of the trAerosol experiment is about a factor of 2 larger than the median HS of the GHG experiment, which is 1.9% per kelvin (mean of 1.7% per kelvin). The observed HS value of 7% per kelvin from the SSM/I data for the period of 1987–2006 is well within the standard deviation of ± 2.6% per kelvin of the mean HS of trAerosol. The 20-yr HS distributions for the GHG and trAerosol simulations are shown in Fig. 4. As expected, F4
the GHG distribution is very similar to the twenty-first-century HS distribution in Fig. 3, which is dominated by greenhouse gas warming. Most of the hydrological sensitivities fall between 0% and 3% per kelvin, which is much smaller than the CC rate. Note that, similar to the twenty-first-century distributions (Fig. 3), about 6% of the 20-yr global P trends in GHG are negative despite positive SAT trends for these periods, which indicates large interdecadal variability. This is not the case for trAerosol, for which the entire HS distribution is positive and substantially broader than GHG, with approximately 23% of the 20-yr sensitivities above the CC rate. Thus, the analysis of hydrological sensitivity and its interdecadal variability indicates different characteristics for different forcing agents.

5. Thermodynamic control of precipitation changes

To close the atmospheric water budget P must equal E in a global, annual sense, and changes in precipitation δP must equal changes in evaporation δE at the surface. Further, precipitation changes δP are accompanied by anomalous release of latent heat δQ_{lat} resulting from phase transition. Hence, long-term global precipitation changes, which are discussed here, are linked to changes in the surface energy budget as follows:

$$L\delta P = L\delta E = \delta Q_{\text{lat}} = \delta R_{\text{srf}} - \delta Q_{\text{sen}} - \delta M. \quad (1)$$

Here, L is the energy of phase transition, δR_{srf} is the net radiative energy change at the surface, δQ_{sen} is the sensible heat change, and δM is the ocean and land heat uptake (plus a small contribution from changes in melting of snow and ice). We introduce a modified Bowen ratio B^* that links the global-mean changes of sensible heating δQ_{sen} and latent heating δQ_{lat} as follows:

$$B^* \equiv \delta Q_{\text{sen}}/\delta Q_{\text{lat}}. \quad (2)$$

Equation (1) can then be rewritten as

$$\delta P = \frac{\delta R_{\text{srf}} - \delta M}{L(1 + B^*)}. \quad (3)$$

On decadal time scales the ocean and land heat uptake δM is equal to the radiative imbalance at the top of

JOBNAME: JCLI 00#0 2009 PAGE: 9 SESS: 8 OUTPUT: Tue Mar 31 20:34:01 2009 Total No. of Pages: 11
/ams/jcli/0/jcli2472

the atmosphere δR_{TOA} (Hansen et al. 2005a). Replacing δM with δR_{TOA} in Eq. (3) and dividing both sides of the equation by the global-mean surface air temperature change δT leads to

$$L(1 + B^*)\frac{\delta P}{\delta T} = \frac{\delta R_{\mathrm{srf}}}{\delta T} - \frac{\delta R_{\mathrm{TOA}}}{\delta T}. \quad (4)$$

Thus, the modified energy balance in Eq. (4) links the hydrological sensitivity $\delta P/\delta T$ to the climate sensitivity, here the global surface air temperature response to the adjusted TOA radiative imbalance $\delta R_{\mathrm{TOA}}/\delta T$. This means that HS is linearly related to the difference of the surface and TOA radiative imbalances, with a slope determined by the modified Bowen ratio B^*.

F5 Figure 5 illustrates this linear behavior in the GISS_ER model simulations. Shown is the scatterplot of the global overlapping 20-yr trends of monthly precipitation anomalies for the GHG (red asterisks) and the trAerosol (blue asterisks) simulations against the trends of the differences of surface-minus-TOA net radiative flux monthly anomalies. The slope of the linear regression line through all of the data (i.e., GHG and trAerosol) is 12.7 mm yr^{-1} (W m^{-2}) $^{-1}$. This slope corresponds to a B^* of -0.0065, which means that 20-yr sensible heat flux trends are significantly smaller and anticorrelated to latent heat flux trends for the same time periods. Recalculating the slope for each experiment separately, we find modified Bowen ratios of -0.30 for GHG and $+0.40$ for trAerosol. Hence, for the GHG experiment the sensible heat flux trends tend to be one-third in magnitude and anticorrelated to the latent heat flux trends, whereas in the trAerosol case sensible and latent heat flux trends tend to be correlated.

6. Summary and conclusions

A new satellite-derived analysis of global precipitation (W07) detected an increase of global-mean P of 13.2 ± 4.8 mm per decade ($1.4 \pm 0.5\%$ per decade) over the period from July 1987 through August 2006. With a surface air temperature increase of 0.2 K per decade, this trend amounts to a hydrological sensitivity of 7% per kelvin, which is close to the Clausius–Clapeyron rate that describes the dependence of water vapor saturation pressure on temperature. Our analysis of two newly available ocean evaporation datasets for January 1987–December 2004 indicates an increase in global-mean E that is consistent with the W07 global-mean P trend within the limits of data uncertainty. The linear trends in global E are significant at the 95% confidence level with 16 ± 8 mm per decade for the OAFlux estimates and 45 ± 35 mm per decade for the HOAPS3 estimates. A strong drop in E following the Mount Pinatubo volcanic eruption in June 1991 is a prominent feature in HOAPS3 but not in the OAFlux dataset. Differences in the choice of input data may cause this discrepancy, and further, more detailed investigation is needed.

Our analysis confirms the W07 result that state-of-the-art climate models underestimate the observed 7% per kelvin hydrological sensitivity during 1987–2006. We show in this study, nonetheless, that CMIP3 coupled atmosphere–ocean climate models can produce an HS this large on 20-yr time scales. About 12% of 20-yr time periods of the twentieth-century climate simulations are characterized by HS equal to or larger than the CC rate. However, the average HS for all 20-yr periods in this century (and in the twenty-first-century simulations of the CMIP3 models) is much smaller, being about 1.4% per kelvin. (Note that 6% of the 20-yr intervals in the twenty-first-century simulations exhibit global warming concurrent with declining precipitation.) Thus, the global P change during a given 20-yr period may not be representative of the changes that will occur on longer time scales.

The main difference between the twentieth and twenty-first century in the models is the dominance of the greenhouse gas forcing over the tropospheric aerosol forcing in the current century. The analysis of special GISS_ER climate runs shows that HS of simulations with only twentieth-century tropospheric aerosol forcing (trAerosol) can be up to 5 times as large as the HS of simulations forced by twentieth-century GHGs only. The median 20-yr HS is 4% per kelvin for the trAerosol experiment and 2% per kelvin for the GHG experiment. The HS distribution of the trAerosol experiment is substantially broader, with 23% of the 20-yr time intervals characterized by an HS above the CC rate.

We further investigated the relationship between hydrological sensitivity and climate sensitivity (here the ratio of TOA radiative imbalance to global-mean surface air temperature change over a multiannual time period). In a global, long-term mean sense, hydrological sensitivity can be related to the energy imbalance of the atmosphere. We show that long-term variations in surface-minus-TOA radiative imbalance (atmospheric radiative energy imbalance) correlate linearly with precipitation variations. The strength of this linear relationship (i.e., the slope) is determined by the modified Bowen ratio B^*, which is here defined as sensible heat flux changes divided by latent heat flux changes at the surface. (Note that the Bowen ratio is generally defined as average sensible heat flux divided by average latent heat flux.) We show that the GISS_ER model reproduces this analytically derived linear relationship very well. Latent heat changes and sensible heat changes in the model are anticorrelated in the GHG experiment and correlated in the trAerosol experiment (B^* of -0.3 and 0.4,

respectively). When data from both experiments are combined, latent heat flux changes are significantly larger than and anticorrelated with sensible heat flux changes.

Equation (4) states that the hydrological sensitivity is controlled by changes in the atmospheric radiative energy imbalance. This energy imbalance exists largely because the atmosphere is relatively transparent to SW radiation, and thus atmospheric SW absorption is smaller than the net LW emission from the atmosphere. Therefore, changes in the atmospheric radiative energy imbalance should be proportional to changes in the SW transmissivity of the atmosphere. Because clouds and aerosols significantly affect the SW transmissivity by reflecting and absorbing incoming SW radiation (e.g., Liepert 2002; Liepert and Tegen 2002; Kim and Ramanathan 2008), we expect them generally to produce a stronger HS than greenhouse gases, which have comparatively little effect on SW transmission. This is supported by our analysis of the GISS_ER GHG and trAerosol experiments. In the latter experiment, changes in both surface sensible heat flux and latent heat flux act to counter the changes in atmospheric radiative energy imbalance (i.e., positive B^*), whereas in GHG sensible and latent heat flux changes oppose one another (negative B^*).

Based on our model analysis, we find that an increase in the difference between global surface and TOA net radiation of 0.7 W m^{-2} per decade would be needed to account for the observed precipitation increase of 13 mm yr^{-1} per decade from 1987 to 2006. We investigated global-mean radiative flux anomalies for the time period from July 1987 to December 2005 using the Surface Radiation Budget (SRB) dataset from the NASA Langley Research Center Atmospheric Sciences Data Center (available online at http://eosweb.larc.nasa.gov/PRDOCS/srb/table_srb.html) and found that the difference between surface and TOA net radiation increased by 0.8 W m^{-2} per decade [see also Zhang et al. (2007) for an alternative dataset]. However, even for the deseasonalized monthly anomalies, the standard deviation of this estimate is about 2 W m^{-2} per decade, signifying large uncertainty in the radiative flux measurements and thus precluding any definitive conclusion about whether the flux changes are consistent with the observed P change.

The mid-1980s and mid-1990s saw a decrease in stratospheric aerosol injected by the eruptions of the volcanoes El Chichón (1982) and Mount Pinatubo (1991). Global reductions in anthropogenic aerosol optical depths (Mishchenko et al. 2007) and decreases in global cloudiness (Wielicki et al. 2002; Romanou et al. 2007) resulting from less frequent El Niño events were also recently observed by satellites. These cloud and aerosol changes induced a ''brightening'' trend that may have contributed to the rapid increase in global P observed during the past two decades (see also Trenberth and Dai 2007). Detection of ''dimming and brightening'' trends, however, is still subject of ongoing investigation (see Hinkelmann et al. 2008, manuscript submitted to *J. Geophys. Res.*). We also suggest that more observational studies are needed to evaluate the relationship between hydrological sensitivity and the radiative forcing of climate, as we have done here using the GISS model.

Acknowledgments. This work was sponsored by NASA MAP Program Grant NNG06GC66G. We thank Reto Ruedi and Ken Lo for providing the NASA GISS model simulations. We acknowledge the modeling groups for making their model output available for analysis, the Program for Climate Model Diagnosis and Intercomparison (PCMDI) for collecting and archiving these data, and the WCRP's Working Group on Coupled Modeling (WGCM) for organizing the model data analysis activity. The WCRP CMIP3 multimodel dataset is supported by the Office of Science, U.S. Department of Energy. We further thank L. Yu and R. A. Weller from Woods Hole Oceanographic Institution for making available the OAFlux data and the Hamburg Ocean–Atmosphere Parameters and Fluxes from Satellite Data (HOAPS) group of the University of Hamburg and Max-Planck Institute in Hamburg for providing the HOAPS3 data. We also thank the NASA Langley Research Center Atmospheric Sciences Data Center GEWEX/SRB Project, which provided the radiation data.

REFERENCES

Adler, R. F., and Coauthors, 2003: The Version-2 Global Precipitation Climatology Project (GPCP) monthly precipitation analysis (1979–present). *J. Hydrometeor.,* **4,** 1147–1167.

——, G. Gu, J.-J. Wang, G. J. Huffman, S. Curtis, and D. Bolvin, 2008: Relationships between global precipitation and surface temperature on interannual and longer time scales (1979–2006). *J. Geophys. Res.,* **113,** D22104, doi:10.1029/2008JD010536.

Allan, R. P., and B. J. Soden, 2007: Large discrepancy between observed and simulated precipitation trends in the ascending and descending branches of the tropical circulation. *Geophys. Res. Lett.,* **34,** L18705, doi:10.1029/2007GL031460.

Allen, M. R., and W. J. Ingram, 2002: Constraints on future changes in climate and the hydrologic cycle. *Nature,* **419,** 224–232.

Andersson, A., S. Bakan, K. Fennig, H. Grassl, C.-P. Klepp, and J. Schulz, 2007: Hamburg Ocean Atmosphere Parameters and Fluxes from Satellite Data—HOAPS-3 monthly mean. World Data Center for Climate, doi:10.1594/WDCC/HOAPS3_MONTHLY.

Boer, G. J., 1993: Climate change and the regulation of the surface moisture and energy budgets. *Climate Dyn.,* **8,** 225–239.

Chen, J., B. E. Carlson, and A. D. Del Genio, 2002: Evidence for strengthening of the tropical general circulation in the 1990s. *Science,* **295,** 838–841.

Fairall, C. W., E. F. Bradley, J. E. Hare, A. A. Grachev, and J. B. Edson, 2003: Bulk parameterization of air–sea fluxes: Updates and verification for the COARE algorithm. *J. Climate,* **16,** 571–591.

Feichter, J., U. Lohmann, B. Liepert, and E. Roeckner, 2004: Nonlinear aspects of the climate response to greenhouse gas and aerosol forcing. *J. Climate,* **17,** 2384–2398.

Gillett, N. P., A. J. Weaver, F. W. Zwiers, and M. F. Wehner, 2004: Detection of volcanic influence on global precipitation. *Geophys. Res. Lett.,* **31,** L12217, doi:10.1029/2004GL020044.

Gu, G., R. F. Adler, G. J. Huffman, and S. Curtis, 2007: Tropical rainfall variability on interannual-to-interdecadal and longer time scales derived from the GPCP monthly product. *J. Climate,* **20,** 4033–4046.

Hansen, J., and Coauthors, Earth's energy imbalance: Confirmation and implications. *Science,* **308,** 1431–1435, doi:10.1126/science.1110252.

——, and Coauthors, 2005b: Efficacy of climate forcings. *J. Geophys. Res.,* **110,** D18104, doi:10.1029/2005JD005776.

——, and Coauthors, 2007: Climate simulations for 1880–2003 with GISS modelE. *Climate Dyn.,* **29,** 661–696, doi:10.1007/s00382-007-0255-8.

Held, I. M., and B. J. Soden, 2006: Robust responses of the hydrological cycle to global warming. *J. Climate,* **19,** 5686–5699.

Hinkelmann, L. M., P. Stackhouse Jr., B. A. Wielicki, T. Zhang, and S. R. Wilson, 2008: Surface insolation trends from satellite and ground measurements: Comparisons and challenges. AU4 *J. Geophys. Res.,* submitted.

Kim, D., and V. Ramanathan, 2008: Solar radiation budget and radiative forcing due to aerosols and clouds. *J. Geophys. Res.,* **113,** D2203, doi:10.1029/2007JD008434.

Koch, D., Transport and direct radiative forcing of carbonaceous and sulfate aerosols in the GISS GCM. *J. Geophys. Res.,* **106,** 20 311–20 332.

Liepert, B. G., 2002: Observed reductions in surface solar radiation in the United States and worldwide from 1961 to 1990. *Geophys. Res. Lett.,* **29,** 1421, doi:10.1029/2002GL014910.

——, and I. Tegen, 2002: Multidecadal solar radiation trends in the United States and Germany and direct tropospheric aerosol forcing. *J. Geophys. Res.,* **107,** 4153, doi:10.1029/2001JD000760.

——, J. Feichter, U. Lohmann, and E. Roeckner, 2004: Can aerosols spin down the water cycle in a warmer and moister world? *Geophys. Res. Lett.,* **31,** L06207, doi:10.1029/2003GL019060.

Lorenz, D. J., and E. T. DeWeaver, The response of the extratropical hydrological cycle to global warming. *J. Climate,,* **20,** 3470–3484.

Mishchenko, M. I., I. V. Geogdzhayev, W. B. Rossow, B. Cairns, B. E. Carlson, A. A. Lacis, L. Liu, and L. D. Travis, 2007: Long-term satellite record reveals likely recent aerosol trend. *Science,* **315,** 1543, doi:10.1126/science.1136709.

Mitchell, J. F. B., C. A. Wilson, and W. M. Cunnington, 1987: On CO_2 climate sensitivity and model dependence of results. *Quart. J. Roy. Meteor. Soc.,* **113,** 293–322.

Romanou, A., B. Liepert, G. A. Schmidt, W. B. Rossow, R. A. Ruedy, and Y.-C. Zhang, 2007: 20th century changes in surface solar irradiance in simulations and observations. *Geophys. Res. Lett.,* **34,** L05713, doi:10.1029/2006GL028356.

Santer, B. D., and Coauthors, 2000a: Interpreting differential temperature trends at the surface and in the lower troposphere. *Science,* **287,** 1227–1232.

——, T. M. L. Wigley, J. S. Boyle, D. J. Gaffen, J. J. Hnilo, D. Nychka, D. E. Parker, and K. E. Taylor, 2000b: Statistical significance of trends and trend differences in layer-average atmospheric temperature time series. *J. Geophys. Res.,* **105,** 7337–7356.

Solomon, S., D. Qin, M. Manning, M. Marquis, K. Averyt, M. M. B. Tignor, H. L. Miller Jr., and Z. Chen, Eds., 2007: *Climate Change 2007: The Physical Science Basis*. Cambridge University Press, 996 pp.

Trenberth, K. E., and A. Dai, 2007: Effects of Mount Pinatubo volcanic eruption on the hydrological cycle as an analog of geoengineering. *Geophys. Res. Lett.,* **34,** L15702, doi:10.1029/2007GL030524.

——, J. Fasullo, and L. Smith, 2005: Trends and variability in column-integrated atmospheric water vapor. *Climate Dyn.,* **24,** 741–758, doi:10.1007/s00382-005-0017-4.

——, and Coauthors, 2007: Observations: Surface and atmospheric climate change. *Climate Change 2007: The Physical Science Basis*, S. Solomon et al., Eds., Cambridge University Press, 235–336.

Wentz, F. J., L. Ricciardulli, K. Hilburn, and C. Mears, 2007: How much more rain will global warming bring? *Science,* **317,** 233–235.

Wielicki, B. A., and Coauthors, 2002: Evidence for large decadal variability in the tropical mean radiative energy budget. *Science,* **295,** 841–844.

Xie, P., and P. Arkin, 1998: Global monthly precipitation estimates from satellite-observed outgoing longwave radiation. *J. Climate,,* **11,** 137–164.

Yin, X., A. Gruber, and P. Arkin, 2004: Comparison of the GPCP and CMAP merged gauge–satellite monthly precipitation products for the period 1979–2001. *J. Hydrometeor.,* **5,** 1207–1222.

Yu, L., and R. A. Weller, 2007: Objectively analyzed air–sea heat fluxes for the global ice-free oceans (1981–2005). *Bull. Amer. Meteor. Soc.,* **88,** 527–539.

Zhang, Y., W. B. Rossow, P. Stackhouse Jr., A. Romanou, and B. A. Wielicki, 2007: Decadal variations of global energy and ocean heat budget and meridional energy transports inferred from recent global data sets. *J. Geophys. Res.,* **112,** D22101, doi:10.1029/2007JD008435.